

Optical Engineering

OpticalEngineering.SPIEDigitalLibrary.org

Preliminary research on focal plane calibration method in LAMOST based on flexible planar target

Lianpo Wang
Ye Zhu
Xiang Lu
Yonggang Gu
Chao Zhai

Preliminary research on focal plane calibration method in LAMOST based on flexible planar target

Lianpo Wang,^{a,†} Ye Zhu,^{a,†} Xiang Lu,^a Yonggang Gu,^{b,*} and Chao Zhai^b

^aUniversity of Science and Technology of China, Department of Precision Machinery and Precision Instrumentation, Hefei, Anhui Province, China

^bUniversity of Science and Technology of China, Experiment Center of Engineering and Material Science, Hefei, Anhui Province, China

Abstract. In the large sky area multiobject optical fiber spectroscopy telescope project, to capture the spectrum of a particular object, the optical fiber positioner must position the optical fiber end face to a specified location on the focal plane. The accuracy of the optical fiber positioner is guaranteed by feedback from photogrammetry. Photogrammetry accuracy is based on accurate calibration. However, given the complexities in the optical fiber focal plane and the optical fiber positioner, the accurate standard point is considerably difficult to obtain, which results in insufficient calibration accuracy. To solve this problem, a convenient calibration method based on the combination of small, planar targets is proposed. In this method, each optical fiber positioner positions the optical fiber to several designed locations, which are relatively accurate. These points form a high-precision, two-dimensional point array that can be used as the planar target. In this manner, each optical fiber positioner can be regarded as a small, high-precision planar target. All small, high-precision planar targets are assembled to form the flexible planar target, which is used for calibration. The experimental result indicates that this method is highly accurate and can be applied in focal plane calibration. © The Authors. Published by SPIE under a Creative Commons Attribution 3.0 Unported License. Distribution or reproduction of this work in whole or in part requires full attribution of the original publication, including its DOI. [DOI: [10.1117/1.OE.57.5.054109](https://doi.org/10.1117/1.OE.57.5.054109)]

Keywords: flexible planar target; calibration; photogrammetry; large sky area multiobject optical fiber spectroscopy telescope.

Paper 180353 received Mar. 5, 2018; accepted for publication May 1, 2018; published online May 21, 2018.

1 Introduction

Large sky area multiobject optical fiber spectroscopy telescope (LAMOST) is one of the world's largest optical fiber spectroscopy telescopes, which are a kind of comprehensive, large-scale optical instrument used to record the spectrum of numerous stars.¹ The LAMOST simultaneously observes and records the spectrum of 4000 stars through 4000 optical fibers, which are driven by high-precision optical fiber positioners on the focal plane. Each optical fiber positioner, which contains two noncoaxial motors, has two degrees of freedom. Each optical fiber positioner can also position the optical fiber anywhere within a 33-mm-diameter circular patrol region. In order to capture the spectrum of a particular object, the optical fiber positioner requires multiple iterations to position the optical fiber end face precisely to a target location in its corresponding patrol region. The required positioning accuracy of each optical fiber is $\sigma \leq 40 \mu\text{m}$. Position feedback and closed-loop control are necessary to compensate positioning errors. Therefore, the metrology of optical fiber position is mandatory. Photogrammetry is selected as the metrology technology in this research because of its ability to measure the position of numerous targets simultaneously. In photogrammetry, the calibration of the spatial relationship between the camera and the optical fiber on the focal plane is fundamental.

Given that the optical fiber positioners are densely distributed on the focal plane, additional control points cannot be placed. Researchers have developed several calibration

methods. Liu et al.² assumed that the center of the optical fiber positioners coincides with the center of the installation hole. The three-dimensional (3-D) coordinate of this hole under the global coordinate system is designed and known. The focal plane can be calibrated using the 3-D position of the installation hole. This method is feasible but does not take into consideration the assembly errors, which can lead to unacceptable calibration error. Fisher et al.³ installed the optical fiber positioners on a fixture containing several reference optical fibers in order to test the positioning accuracy of the optical fiber positioned. The reference optical fiber and the optical fiber to be tested are imaged by a camera to determine the position of the optical fiber. However, this method can only be used for offline detection; online testing does not allow the presence of a reference optical fiber. Other researchers also proposed several calibration methods for the optical fiber focal plane. For example, excellent calibration is achieved by upgrading the hardware of the camera.⁴⁻⁸ Some researches on the calibration of optical fiber focal plane were also conducted without taking into consideration the assembly error.⁹⁻¹¹

To solve this problem, this article draws on the characteristic that optical fiber positioner can precisely carry out the relative displacement. In this method, each optical fiber positioner positions the optical fiber to 16 designed locations that are relatively accurate. These points form a high-precision, two-dimensional point array that can be used as the small, high-precision planar target. The proposed method does not use the absolute position of the optical fiber positioner, so the effect of assembly errors on the calibration is avoided. To calibrate the entire focal plane using these small planar targets, an improved calibration method based on flexible

*Address all correspondence to: Yonggang Gu, E-mail: ygggu@ustc.edu.cn

[†]These authors contributed equally to this work.

planar target (FPT) method is also proposed. Multiple small, high-precision targets are assembled to form the FPT, which is used as a large, planar target.¹²⁻¹⁷

The remaining part of this paper is organized as follows: in Sec. 2, the camera model is described. Focal plane and small planar target models are presented in Sec. 3. Section 4 describes the calibration algorithm based on FPT method. Section 5 provides the experimental results. Finally, Sec. 6 concludes the paper.

2 Camera Projection Model

Under linear assumption, the relationship between the point (u, v) under camera coordinate system and (X, Y, Z) under the world coordinate system satisfies the following equation:

$$\begin{bmatrix} u \\ v \\ 1 \end{bmatrix} = s \begin{bmatrix} F_x & \beta & C_x & 0 \\ 0 & F_y & C_y & 0 \\ 0 & 0 & 1 & 0 \end{bmatrix} \begin{bmatrix} R & T \\ 0^T & 1 \end{bmatrix} \begin{bmatrix} X \\ Y \\ Z \\ 1 \end{bmatrix} \quad (1)$$

$$= s \cdot A \cdot [R \ T] \cdot q_W = H \cdot q_W.$$

In this equation, the homomorphic matrix H includes the nonzero scale factor s , intrinsic parameter A , and extrinsic parameter $[R \ T]$. Five parameters are used in intrinsic parameter A . F_x and F_y are the scale factors along the image axes u and v , and (C_x, C_y) is the principal point. Parameter β is the skew of the two image axes. $[R \ T]$ represents the rotation matrix and the translation vector from the world coordinate frame to the camera coordinate frame.

Given the processing, installation, and other reasons, the camera lens is often distorted, and spatial projection does not strictly follow the perspective projection imaging model. Camera lens distortion can be classified as radial distortion, tangential distortion, centrifugal distortion, and thin prism distortion. The distortion model used in this paper is the Plumb Bob model.¹⁸ The distortion correction equation is as follows:

$$\begin{cases} x_{corrected} = (1 + k_1 r^2 + k_2 r^4 + k_3 r^6) * x + 2k_3 xy + k_4 (r^2 + 2x^2) \\ y_{corrected} = (1 + k_1 r^2 + k_2 r^4 + k_3 r^6) * y + 2k_4 xy + k_3 (r^2 + 2y^2) \end{cases} \quad (2)$$

Suppose $\begin{bmatrix} x \\ y \end{bmatrix} = \begin{bmatrix} \tilde{x} - C_x \\ \tilde{y} - C_y \\ F_x \\ F_y \end{bmatrix}$, $r^2 = x^2 + y^2$, where

$(x_{corrected}, y_{corrected})$ represent the corrected coordinates, (x, y) is the normalized image coordinate, (\tilde{x}, \tilde{y}) is based on the central perspective projection model given the ideal pixel, and $k_1 - k_5$ is the distortion factor.

3 Focal Plane and Small Planar Target Model

The focal plane is a spherical crown with a diameter of 1.75 m and a curvature radius of ~19.88. A total of 4000 optical fiber positioners uniformly plugged in the focal plane are shown in Fig. 1. As shown in Fig. 2, the Z-axis direction of the world coordinate system is the normal direction at point O of the focal plane. The $X - Y$ plane coincides with the tangent plane at O point. The error of the optical fiber in the Z-direction is denoted as δ_z , the error in the XY plane is δ_{XY} , and the error on the spherical surface of

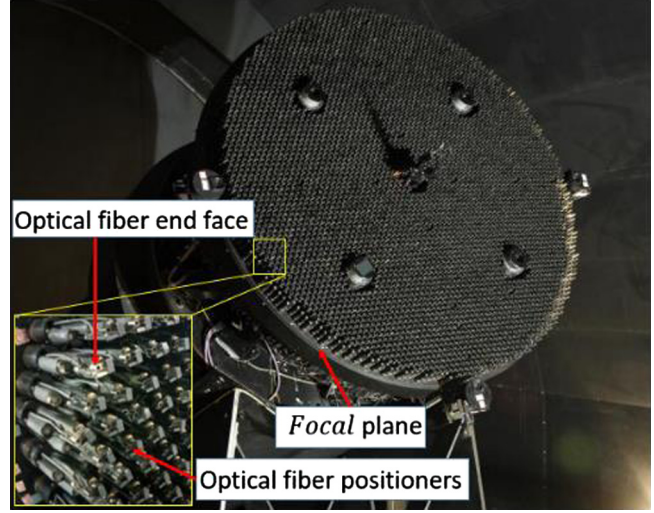


Fig. 1 Physical map of the focal plane.

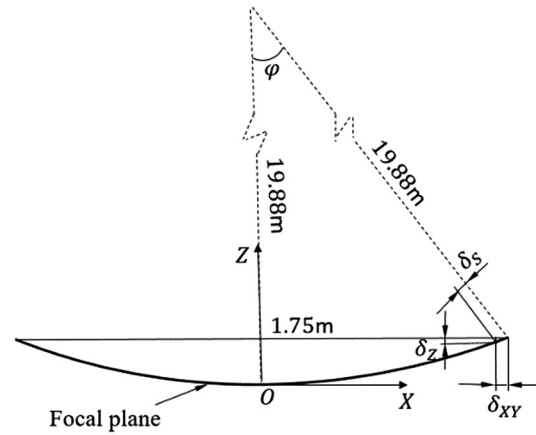


Fig. 2 Focal plane error model.

the focal plane is δ_s . According to the geometric relationship in Fig. 2, the following equations are obtained:

$$\delta_z = \delta_s \sin \phi \approx 0, \quad (3)$$

$$\delta_{XY} = \delta_s \cos \phi \approx \delta_s. \quad (4)$$

Given that angle ϕ is very small, we can assume that $\sin \phi \approx 0$ and $\cos \phi \approx 1$. Evidently, $\delta_z \approx 0$ and $\delta_{XY} \approx \delta_s$. Therefore, the optical fiber end faces positioning error on the focal plane δ_s , which is mainly reflected in δ_{XY} . The Z-direction error δ_z is negligible. Hence, the following error analysis is mainly the analysis on δ_{XY} .

In each observation, 4000 optical fiber positioners drive 4000 optical fibers, so each optical fiber is aligned with a single object. Each optical fiber positioner shows a double-swing mechanism, as shown in Fig. 3. The range of motion of an optical fiber positioner is a 33-mm-diameter circular area driven by two stepper motors. The distance between two adjacent optical fiber positioners is 25.6 mm, and an overlapping area exists between adjacent optical fiber positioners. This area ensures that the observation

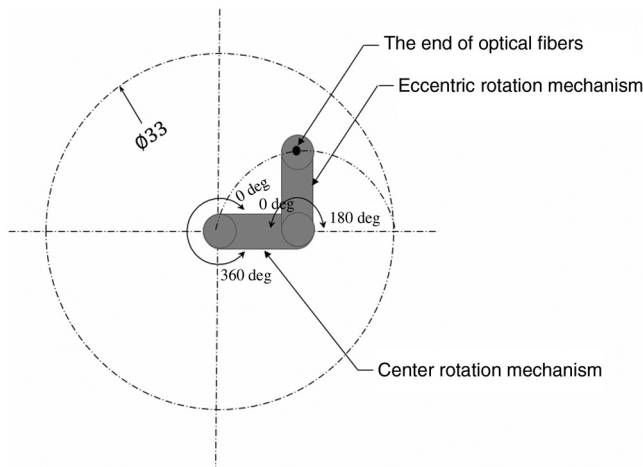


Fig. 3 Optical fiber positioner model.

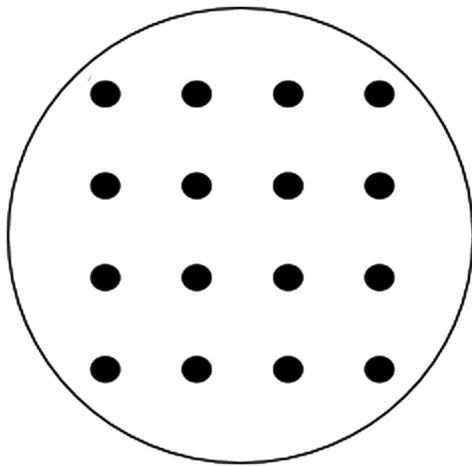


Fig. 4 Small planar target model.

possesses no blind spots and improves the observation efficiency.

Given the increasingly sophisticated stepping motor hardware and software and the use of the piezoelectric ceramic drive instead of the traditional stepper motor applications, optical fiber positioner can precisely carry out the relative movement. Each optical fiber positioner performs precise relative movements for 16 times. Afterward, each optical fiber positioner can be considered a precision small planar target, as shown in Fig. 4. However, the absolute position between each small planar target is unknown due to the assembly error between the optical fiber positioner and the mounting hole on the focal plane.

4 Calibration Principle

In this section, the conversion of each small planar target into FPT is introduced. Then, the calibration method based on FPT is also described in detail. Finally, the optimization model is proposed.

4.1 Flexible Planar Target Model

According to Sec. 3, 4000 small, high-precision planar targets can be obtained from the entire focal plane. As shown in

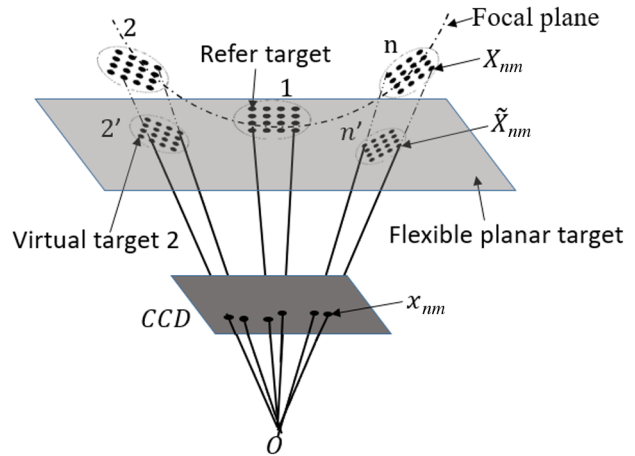


Fig. 5 Schematic diagram of FPT model.

Fig. 5, the small planar target is densely distributed on the focal plane, and the small planar target 1 is selected as the reference datum target. The reference datum target coincides with the FPT. The m 'th feature point on the n 'th small planar target is marked as X_{nm} . The connection between and the optical center O intersects with the CCD plane at x_{nm} and the reference datum target plane at \tilde{X}_{nm} . $O\tilde{X}_{nm}$ and Ox_{nm} are the collinear, that is, the projection relationship of $O\tilde{X}_{nm}$ and Ox_{nm} is consistent. \tilde{X}_{nm} is the corresponding virtual point for X_{nm} . The virtual point \tilde{X}_{nm} can be used instead of X_{nm} for calibration. Similarly, transforming all small planar targets into virtual targets creates the FPT.

The conversion of \tilde{X}_{nm} by X_{nm} is described in the following. The process of obtaining FPT without losing generality will be described using two small planar targets. The small planar target 1 is selected as the reference datum target.

According to Eq. (1), the following equations are obtained:

$$x_{nm} = s_n \cdot A \cdot [R_n \ T_n] \cdot X_{nm}, \quad (5)$$

$$x_{nm} = s_1 \cdot A \cdot [R_1 \ T_1] \cdot \tilde{X}_{nm}. \quad (6)$$

The integration of these equations is as follows:

$$\begin{aligned} \tilde{X}_{nm} &= \{s_1 \cdot A \cdot [R_1 \ T_1]\}^{-1} \cdot \{s_n \cdot A \cdot [R_n \ T_n]\} \cdot X_{nm} \\ &= U_n \cdot X_{nm}, \end{aligned} \quad (7)$$

where $U_n = \{s_1 \cdot A \cdot [R_1 \ T_1]\}^{-1} \cdot \{s_n \cdot A \cdot [R_n \ T_n]\} = H_1^{-1} \cdot H_n$, so that \tilde{X}_{nm} can be obtained via the coordinates X_{nm} and homomorphic matrices H_n . Similarly, this method can be generalized to construct the FPT with multiple small planar targets.

4.2 Calibration Based on FPT

According to Sec. 4.1, a large FPT can be obtained. This FPT is calibrated using the two-step method. In the first step, assuming that the camera is undistorted, the projection model is a linear model, such as that in Eq. (1). With establishment and solving over determined linear equations, the homomorphic matrix H can be calculated as follows:

$$x_{nm} = H \cdot \tilde{X}_{nm}, H = \begin{bmatrix} h_1 & h_2 & h_3 \\ h_4 & h_5 & h_6 \\ h_7 & h_8 & h_9 \end{bmatrix}. \quad (8)$$

In the second step, with consideration of the distortion factor, we use the distortion model described in Sec. 2 to correct the effects of distortion. After the completion of these two steps, loop iteration is performed until the residual is minimal.

When Eqs. (7) and (8) are combined, the following equation is obtained:

$$x_{nm} = H \cdot U_n \cdot X_{nm}, \quad (9)$$

where H is a homomorphic matrix between the camera and the FPT, which can be obtained from Eq. (8). U_n is the transformation matrix of the n 'th subcalibration plate that can be obtained by Eq. (7). However, the obtained parameters are all initial values and require optimization. The above equation is not strictly satisfied, because there is an error δ

$$\delta = x_{nm} - H \cdot U_n \cdot X_{nm} = x_{nm} - \tilde{x}_{nm}, \quad (10)$$

where \tilde{x}_{nm} is the projection point of point X_{nm} , X_{nm} is the actual imaging point of point X_{nm} . The parameters must be optimized, and the detailed optimization method is discussed in Sec. 4.3. The optimized parameters \tilde{H} and \tilde{U}_n are obtained.

We can rewrite Eq. (9) as follows:

$$X_{nm} = \tilde{U}_n^{-1} \cdot \tilde{H}^{-1} \cdot x_{nm}. \quad (11)$$

When the calibration is completed, the \tilde{U}_n and \tilde{H} values can be obtained. The 3-D position X_{nm} of the optical fiber end surface can be calculated from the pixel coordinate x_{nm} according to the above equation.

4.3 Optimization Model

According to the projection model Eq. (9) and the distortion model Eq. (2), the sum of the reprojection error between the projection point \tilde{x}_{nm} and the actual imaging point x_{nm} is optimized to a minimum. The sum of the reprojection error of all points on the FPT is as follows:

$$f(Z) = \min \sum_{n=1}^N \sum_{m=1}^M d^2(x_{nm}, \tilde{x}_{nm}), \quad (12)$$

where N is the number of small planar targets in the field of view, and M is the number of feature point in each small planar target. The optimization parameter Z contains distortion coefficients $k_1 - k_5$, homomorphic matrix H , and transformation matrix $U_2 - U_n$. The nonlinear optimization problem is solved via the Levenberg–Marquardt algorithm.

5 Experiments

To verify the calibration method proposed in this paper, several experiments were implemented. The experiments were carried out according to the following settings: (1) the camera focal length is 16 mm, (2) the image size is 1040 pixels \times 1040 pixels, (3) the field of view of the camera is about 350 mm \times 350 mm, (4) the measuring distance is about 400 mm, and (5) the camera intrinsic parameter

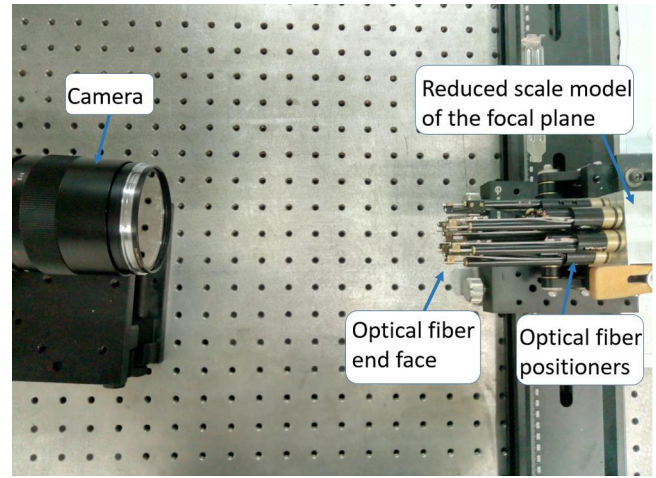


Fig. 6 Physical map of the experimental system.

matrix is $A = \begin{bmatrix} 2963.4 & 0 & 521.4 \\ 0 & 2964.2 & 486.0 \\ 0 & 0 & 1 \end{bmatrix}$. Furthermore,

the distortion factors are $k_1 = -0.009$, $k_2 = 0.241$, $k_3 = -0.000427$, $k_4 = -0.000744$, and $k_5 = 0$. This configuration is only used for validation experiments, not in actual measurement process. These parameters are the internal parameters of the camera, and they are obtained in precalibration experiments using Zhang's algorithm and a precision calibration board. The precalibration obtained these parameters as initial values for optimization; the following experiments did not verify calibration accuracy with these parameters. The accuracy of the calibration method proposed in this paper is verified by solving the error between the measurement position obtained by this method and its true value (measured by a laser tracker).

As shown in Fig. 6, the experimental system is set up on an optical table. The system consists of a high-precision monochrome CCD camera, several optical fiber positioners, and a reduced scale model of the focal plane. The following experiments were carried out to study the effects of three factors on the calibration accuracy, including size of the FPT area, number of small targets, and number of points in each small target.

5.1 Analysis on the Effects of the FPT Area on Calibration Accuracy

The FPT area is the smallest convex polygon that contains all small planar targets, as shown in Fig. 7. The following experiment explores the effects of the FPT area on calibration accuracy.

In this experiment, nine optical fiber positioners were used, and each fiber positioner was subjected to 16 relative movements, then nine small, 4 \times 4 planar targets were obtained. In other words, the FPT used in this experiment consists of nine small planar targets, and the number of feature points in each small planar target is 4 \times 4. In order to explore the effects of the FPT area on calibration accuracy, in these experiments, the FPT area varies from 36 mm \times 36 mm to 120 mm \times 120 mm, respectively. We have calibrated the parameters \tilde{H} and \tilde{U}_n in different FPT areas, and the 3-D position X_{nm} of the optical fiber end

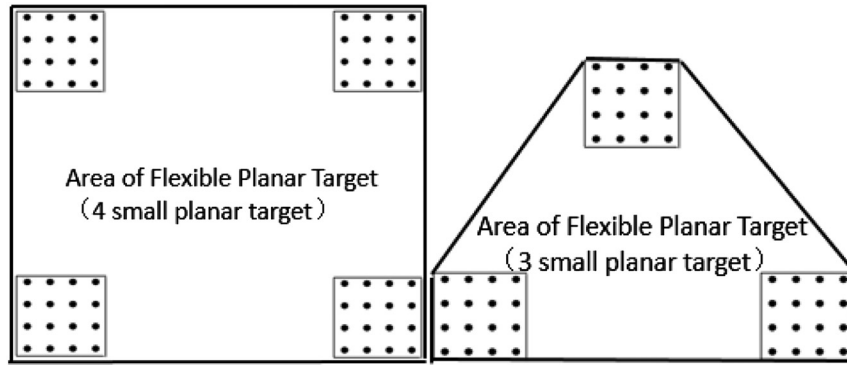


Fig. 7 Schematic diagram of the FPT area.

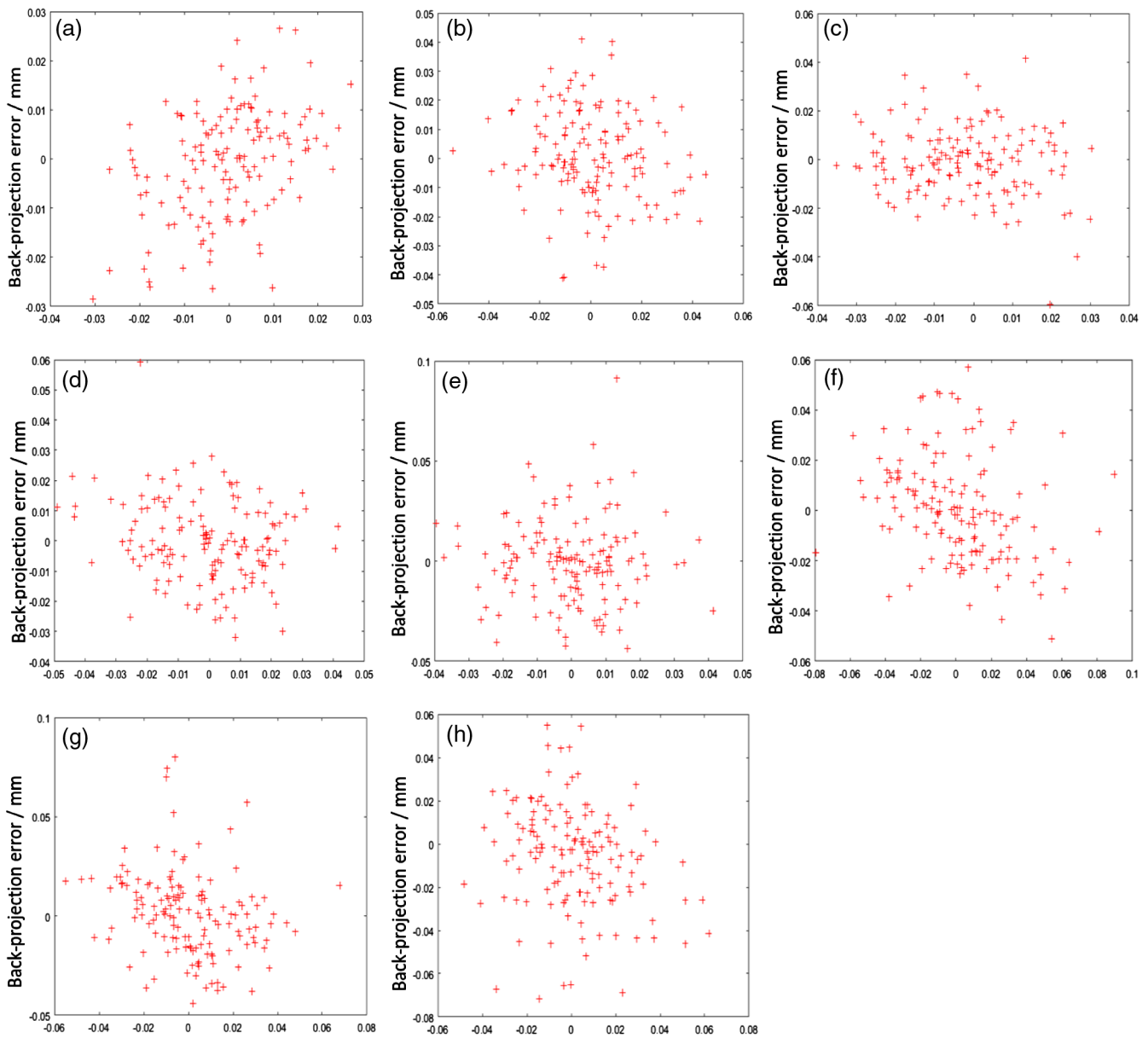


Fig. 8 Backprojection error distribution [when the area of the FPT of (a) to (h) is 36 mm × 36 mm to 120 mm × 120 mm, respectively].

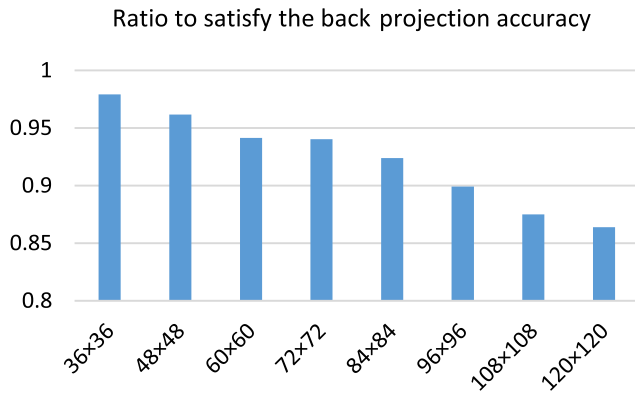


Fig. 9 Effects of the FPT area on calibration accuracy.

surface can be calculated from the pixel coordinate X_{nm} according to Eq. (11) in different \tilde{H} and \tilde{U}_n . Due to image noise, lens distortion, inaccurate model errors, etc., the above-measured X_{nm} and its true value X'_{nm} (detected by the laser tracker) have errors which are called backprojection error.

The backprojection errors of each point are shown in Fig. 8. Figure 9 presents the percentage of points that satisfy the backprojection error of less than $40 \mu\text{m}$. In Fig. 9, the x -coordinate denotes the area of the FPT. It can be concluded from Fig. 9 that the small FPT area results in improved measurement result and vice versa. When each small planar target is distant from each other, the position of each small planar target becomes complex. Optimization may fall into the local optimal solution. Thus, the measurement accuracy decreases slightly.

5.2 Analysis on the Effects of the Number of Small Planar Targets on Calibration Accuracy

The effects of the number of small planar targets on the calibration accuracy are investigated under the condition that the FPT area and the number of feature point are the same. The following comparative experiment ensures that the FPT area is the same as that in Sec. 5.1 experiment: 48×48 , 60×60 , 72×72 , 84×84 , 96×96 , 108×108 , and 120×120 . The number of feature points in each small planar target is 4×4 . The number of small planar targets is increased to 16, which means that the use of 16 optical fiber positioners in the same area.

Figure 10 displays a ratio comparison to satisfy the backprojection error of $<40 \mu\text{m}$ when the number of small planar

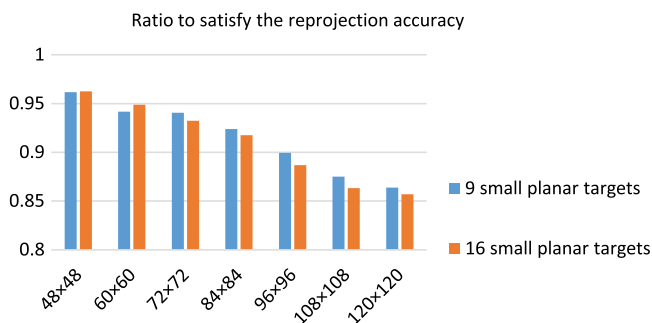


Fig. 10 Effects of the number of small planar targets on calibration accuracy.

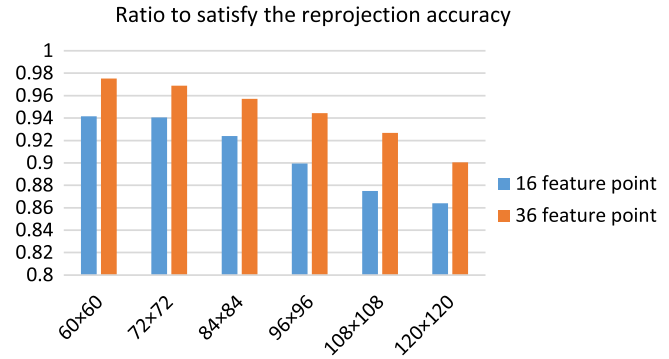


Fig. 11 Effects of the number of points in small planar target on calibration accuracy.

targets is 9 and 16. When the number of small planar target increases to 16, the calibration accuracy slightly decreases. This result can be attributed to that when the number of small planar target increases, the parameters to be optimized also increase correspondingly. The difficulty in optimization also increases.

5.3 Analysis on the Effects of the Number of Points in Each Small Planar Target on Calibration Accuracy

The area of the FPT and the number of small planar targets are the same circumstances, the influence of the number of feature points in each small planar target on the calibration accuracy is investigated. In comparison with the experiment in Sec. 5.1, the number of feature points in each small planar target is changed to 6×6 , which means that each fiber positioner was subjected to 36 relative movements. The number of small planar targets is still 9, and the FPT areas are 60×60 , 72×72 , 84×84 , 96×96 , 108×108 , and 120×120 .

Figure 11 provides a comparison of the experiments in Secs. 5.1 and 5.3. The number of feature points in each small planar target increases to 36, and the calibration accuracy is improved. From the above experiment, it can be concluded that the effect of the number of feature points in each small planar target on camera calibration accuracy is more remarkable than that of the number of small planar targets and the FPT area. Thus, the number of feature points in each small planar target is the key consideration when FPT is used to calibrate the focal plane.

6 Conclusions

This paper presents a focal plane calibration method based on FPT. The use of the characteristic of optical fiber positioner can precisely carry out the relative displacement to avoid the influence of absolute position error, which is caused by the assembly error. This method considers each optical fiber positioner as a small planar target. All small planar targets feature points constitute an FPT. Subsequently, the FPT is used for calibration. The experiments proved the feasibility of using FPT calibration to satisfy the accuracy of $40 \mu\text{m}$ in the proportion of $>85\%$. The effects of various factors on accuracy are also explored. Notably, the method used in this paper uses many nonlinear optimization methods during solving, and its operation time is much longer than those of traditional calibration methods. Future study should

determine how to further improve the computational efficiency of this method, and the extension of this method into practical application of focal plane calibration still needs further study.

References

1. S.-G. Wang et al., "Special configuration of a very large Schmidt telescope for extensive astronomical spectroscopic observation," *Appl. Opt.* **35**(25), 5155–5161 (1996).
2. Z.-G. Liu, J.-Z. Bao, and S.-H. Tang, "Application of least squares fitting circle based on VC in LAMOST," *Mod. Manuf. Eng.* **1**, 94–95 (2008).
3. C. Fisher et al., "Developing engineering model Cobra optical fiber positioners for the Subaru telescope's prime focus spectrometer," *Proc. SPIE* **9151**, 91511Y (2014).
4. S.-Y. Wang et al., "The metrology cameras for Subaru PFS and FMOS," *Proc. SPIE* **8446**, 84464Z (2012).
5. S.-Y. Wang et al., "Metrology camera system of prime focus spectrograph for Subaru telescope," *Proc. SPIE* **9147**, 91475S (2014).
6. W. Saunders et al., "'MOHAWK': a 4000-optical fiber positioner for DESpec," *Proc. SPIE* **8446**, 84464W (2012).
7. C. Fisher et al., "Cobra: a two-degree of freedom optical fiber optic positioning mechanism," in *IEEE Aerospace Conf.*, IEEE (2009).
8. G. Smith et al., "A survey of fiber-positioning technologies," *Proc. SPIE* **5495**, 348–359 (2004).
9. W. Li et al., "Calibration method with separation patterns of a single-camera," *Proc. SPIE* **6269**, 62695I (2006).
10. Y. Gu et al., "A new method for measuring the position of the end of optical fibers for LAMOST," *Proc. SPIE* **7014**, 701444 (2008).
11. Y. Jin et al., "Preliminary study on the measurement system for LAMOST small focal plane optical fiber positioning system," *Proc. SPIE* **6269**, 62693B (2006).
12. L. Yu et al., "A calibration method based on virtual large planar target for cameras with large FOV," *Opt. Lasers Eng.* **101**, 67–77 (2018).
13. Z. Liu et al., "A novel and accurate calibration method for cameras with large field of view using combined small planar targets," *Measurement* **64**, 1–16 (2015).
14. J. Kannala and S. S. Brandt, "A generic camera model and calibration method for conventional, wide-angle, and fish-eye lenses," *IEEE Trans. Pattern Anal. Mach. Intell.* **28**(8), 1335–1340 (2006).
15. J. Huo et al., "An on-line calibration method for camera with large FOV based on prior information," *Optik* **126**(15–16), 1394–1399 (2015).
16. F. Chen, G. M. Brown, and M. Song, "Overview of 3-D shape measurement using optical methods," *Opt. Eng.* **39**(1), 10–22 (2000).
17. S. Zhang and P. S. Huang, "High-resolution, real-time three-dimensional shape measurement," *Opt. Eng.* **45**(12), 123601 (2006).
18. D. C. Brown, "Decentering distortion of lenses," *Photogramm. Eng. Remote Sens.* **32**(3), 444–462 (1966).

Lianpo Wang is a master's student in the Department of Precision Machinery and Precision Instrumentation, University of Science and Technology of China. He mainly engaged in the research of visual measurement, optical precision measurement, etc.

Biographies for the other authors are not available.